Title- Altered histone modifications in *Aedes aegypti* following Rift Valley fever virus exposure

Authors-

Hunter A. Ogg[1,2], Zoey M. Mikol[1,2], David C. King[2], Chad E. Mire[4], Zeyad Arhouma[1,2], Erin Osborne Nishimura[3], Rebekah C. Kading[1,2] and Corey L Campbell[1,2,3*]

[1]Center for Vectorborne Infectious Diseases, [2]Department of Microbiology, Immunology, and Pathology, Colorado State University, Fort Collins, Colorado, 80523, USA. [3]Department of Biochemistry and Molecular Biology, Colorado State University, Fort Collins, Colorado, 80523, USA. [4]United States Department of Agriculture, Agricultural Research Services, National Bio and Agro-defense Facility, Foreign Arthropod-Borne Animal Diseases Research Unit, Manhattan, Kansas, USA

*Corresponding author

Email: corey.campbell@colostate.edu

Keywords-

Mosquito, vector competence, *Culicidae*, chromatin immunoprecipitation sequencing, differential expression, RNA-Seq, ChIP-Seq, histone modifications

Abstract

When arthropod-borne viruses (arboviruses) are delivered to vector mosquitoes in an infectious bloodmeal, viral components interact with host proteins to hijack cells and initiate replication. The extent to which arbovirus infection alters mosquito host transcriptional and genomic regulatory processes is currently unknown. We hypothesized that histone modifications would be altered in mosquitoes exposed to Rift Valley fever virus (RVFV MP12, *Phlebovirus riftense*, family *Phleboviridae*). We interrogated transcriptome and chromatin landscapes in *Aedes aegypti* midguts by performing Cleavage Under Targets and Release Using Nuclease (CUT&RUN), using H3K27ac and H3K9me3 marks. Altered H3K27ac marks were identified following RVFV MP12 exposure, as well as upon bloodfeeding alone. It took several days for differential H3K27ac marks to be associated with differentially expressed genes (DEGs) in RVFV-exposed midguts. H3K27ac peaks showed progressive depletion as infection progressed. Gene set enrichment analysis revealed that immune response transcripts were enriched at 1 and 3 dpf (days post-feeding) but depleted by 7 dpf. Hedgehog/Gli (glioma-associated oncogene homolog) signaling pathway transcripts were depleted, indicating possible viral manipulation of cellular polarization. Moreover, at 7 dpf, 7 of 102 DEGs were proximal to differentially acetylated sites in a pattern expected to favor viral propagation. However, one transcript coding for an antiviral effector (LysM-TLDc domain protein) showed significant depletion of both H3K9me3 and H3K27ac marks. Analysis of midguts after a non-infectious bloodmeal versus sugar-fed controls revealed global changes to H3K27ac and H3K9me3 marks during and following the period of bloodmeal digestion. Differential H3K27ac marks were proximal to one quarter of all DEGs at 1 dpf, consistent with an important role of H3K27ac in bloodmeal digestion. These results demonstrate that H3K27ac and H3K9me3 patterns are altered upon virus exposure in a complex interplay that favors viral replication but is also countered by host responses to limit replication.

Author Summary

Mosquito-borne viruses produce a high disease burden across the globe. Though transgenic mosquitoes are being developed to help mitigate disease transmission, little is known of the ways in which arbovirus infection alters chromatin structure in mosquitoes. Arboviruses typically replicate and assemble on cytoplasmic membranes and have not been traditionally expected to alter processes in the nucleus. Some histone post-translational modifications, such as, e.g. histone 3 lysine 27 acetylation (H3K27ac), are associated with accessible chromatin regions, whereas others, e.g, histone 3 lysine 9 triple-methylation (H3K9me3), are associated with inaccessible chromatin. This work explores these chromatin modifications and the ways in which they are tied to gene expression changes. Multiple lines of evidence presented here support the hypothesis that H3K27ac levels change in RVFV-exposed mosquitoes and are associated with altered gene expression in a manner consistent with viral hijacking of gene expression in the nucleus. In addition, bloodfeeding alone also altered H3K27ac levels at 1-day post-feeding, and over one quarter of differentially expressed genes had changes to H3K27ac marks near transcription start sites, which is consistent with the idea that broad metabolic changes occur to support digestion and egg development.

Introduction

Vector-borne disease outbreaks, particularly those caused by arthropod-borne viruses (arboviruses), have increased in frequency and intensity in recent years[1]. Mosquito-borne viruses are unique in that they must successfully replicate in an alternating fashion among invertebrate and vertebrate hosts. As intracellular pathogens, they interact with host proteins to hijack cellular processes and push metabolic activity in favor of replication and viral assembly.

49 Regardless of whether the host is a mammal or mosquito, selective repression of transcriptional
50 activity occurs[2-4], which is a hallmark of cellular hijacking to enable efficient viral propagation.
51 In vector mosquitoes, immune tolerance and resistance allow viral replication without
52 pathological signs. Virus replication is affected by and, in turn, influences host genomic
53 regulation (reviewed in [5]). Though histone modifications have been best studied with DNA
54 viruses, recent evidence has also implicated histone modifications in the efficacy of RNA virus
55 infection, including flavivirus infection of mosquitoes[6-9]. These alterations could underpin
56 features of host tolerance and resistance in vectors.

57 Histone modifications occur during development [10] across taxa and are also important during
58 the innate immune response[11, 12]. Histone 3 lysine 27 acetylation (H3K27ac) is a trademark
59 of accessible chromatin, which facilitates entry and binding of proteins to initiate transcriptional
60 activation. H3K27ac may also be a marker for enhancer activity and can be perturbed upon
61 pathogen infection[13, 14]. In particular, H3K27ac levels are elevated during Zika virus infection
62 in *Ae. aegypti* cell culture via acetyl transferase CBP activity[6]. In contrast, histone 3 lysine 9
63 triple-methylation (H3K9me3) is associated with heterochromatin or silenced genes (reviewed in
64 [15]); though, during virus infection, specific genes may be derepressed [16]. Though the details
65 of the overall structural features of mosquito chromatin are largely unknown[17], recent efforts
66 have begun to explore distinct elements, such as the importance of histone modifications[18,
67 19]. Other studies used computational approaches to identify *cis* regulatory elements (CREs)
68 that differed between dengue virus susceptible and resistant *Ae. aegypti* strains[20]. Still, much
69 remains to be understood of the role of CREs and chromatin modifications in the vector
70 response to arbovirus infection.

71 Here, we focus on Rift Valley fever virus (RVFV MP12, *Phlebovirus riftense*, family
72 *Phleboviridae*), a vaccine strain for a zoonotic pathogen of concern in sub-saharan Africa[21,
73 22]. Our previous studies established *Ae. aegypti* as a suitable model for study of RVFV-

74 mosquito interactions, including susceptibility to the MP12 vaccine strain[4, 23-25]. Previous
75 vector competence studies led to the hypothesis that *Ae. aegypti* mounts an effective innate
76 immune response against RVFV compared to the much more competent vector, *Culex tarsalis*,
77 as evidenced by viral infection kinetics and differential expression of a key signaling gene,
78 *dishevelled* [4, 23]. In nature, *Ae. aegypti* has expanded its range, which is of concern for
79 spread of mosquito-borne viruses in the US and Europe[26-28].
80
81 To define the relationship between gene expression changes and genomic regulatory regions in
82 arbovirus-infected mosquitoes, we chose to characterize H3K27ac and H3K9me3 histone
83 modifications in midguts of RVFV-MP12-exposed *Ae. aegypti* adult females and compare them
84 to gene expression(Fig 1). Midguts are often the first site of arbovirus replication in vector
85 mosquitoes. Analysis of chromatin marks in mosquito tissues is made possible by recent
86 advances in chromatin immunoprecipitation sequencing, specifically Cleavage Under Targets
87 and Release Using Nuclease (CUT&RUN). This technique and similar approaches require
88 substantially less biological material and have improved signal-to-noise, compared to traditional
89 chromatin immunoprecipitation methods[29-31](Fig 1B). Midgut gene expression changes that
90 occur following exposure to RVFV MP12 were paired with companion analyses of mosquitoes
91 that had received a bloodmeal alone compared to sugar-fed controls. We followed up these
92 studies with interrogation of H3K27ac and H3K9me3 signatures. Our initial hypothesis was
93 bloodfeeding induces gene expression and associated chromatin modifications that set the
94 metabolic foundation for successful arbovirus infection [32]. Moreover, we also predicted
95 histone modifications would be altered following exposure to RVFV MP12 in a manner that
96 favors viral hijacking of host processes, as evidenced by functional roles of differentially
97 expressed genes. We focus first on the changes that occur following RVFV exposure and follow
98 up with the control experiments.

99

100 **Figure 1 legend. CUT&RUN enables capture of histone modifications.** A. Two major
101 experiments were done, RVFV MP12 vs bloodfed (RVFV v BF) or bloodfed vs sugar-fed (BF v
102 SF) at 1, 3, or 7 dpf. Pools of 20 midguts were used for each sample in triplicate biological
103 replicates of CUT&RUN or RNA-Seq. CUT&RUN libraries with inserts <55 nts were removed
104 from analysis. DNA Peaks from merged libraries were called against input controls. B. General
105 overview of CUT&RUN procedure shows that fixed midguts were bound to magnetic beads
106 coated with concanavalin A (green), permeabilized with digitonin, and treated with antibodies
107 specific for H3K27Ac or H3K9me3. Protein A/G- micrococcal nuclease fusion protein cleaves
108 DNA at antibody binding sites for release into the supernatant, then subjected to purification and
109 library preparation. Created in BioRender. (2026) https://BioRender.com/9y5ab72 C.
110 Representative mosquito titers from RVFV-exposed whole mosquitoes collected at 7 dpf. Top
111 row- Infection rates of mosquitoes shown in graph. Bottom row- Infection rates determined from
112 representative carcasses following removal of midguts for CUT&RUN.
113
114

115 # Results

116 ## Gene expression upon RVFV exposure

117 To gain insight into transcriptional profiles following RVFV-MP12 exposure, *Ae. aegypti* were
118 provided an infectious oral bloodmeal, and pooled midguts were processed for RNA-Seq at 1, 3,
119 and 7 days post-feeding (Fig 1A, S1 Table, S1 Fig). Viral bloodmeal titers were 6.9–7.8 log10
120 plaque-forming units (PFU) per ml. Virological confirmation showed that 50% of whole
121 mosquitoes carried infectious virus at 7 days post-feeding (dpf), and a representative set of

122 carcasses showed that about 28% of mosquitoes had disseminated infections (Fig 1C). For the
123 RVFV v bloodfed (BF) comparison at 1 dpf, virus-exposed midgut pools had 94 differential
124 expressed genes (DEGs, FDR <0.10, Fig 2, S2 Table) compared to blood-fed controls. Gene
125 set enrichment analysis (GSEA) using our custom annotation was done to calculate the
126 normalized enrichment score (NES) for each functional category across all the collection times
127 (S3 Table)[33]. NES analysis indicated that overall signaling and immune response genes were
128 enriched at 1 dpf, as was the broad category of replication, (DNA) repair, transcription,
129 translation [34]. As the infection progressed, by 3 dpf, there were 2023 total DEGs. This
130 functional category continued to be enriched, along with cytoskeletal and structural, immune
131 and proteolytic pathways (Fig2B, S2 Fig, S3 Table). By 7 dpf, 102 DEGs were differentially
132 expressed in the RVFV-exposed group, with 71 DEGs depleted, and just 31 transcripts enriched
133 over BF controls (Fig 2, S2 Table). Custom GSEA analysis indicated that replication, (DNA)
134 repair, transcription, translation transcript categories were still over-represented in virus-
135 exposed midguts (S3 Table), which would be consistent with continued viral replication at this
136 timepoint. However, immune response, proteolysis and metabolic functional categories were
137 significantly under-represented, consistent with select transcriptional repression expected during
138 viral hijacking[35, 36].

139 GSEA analyses are often limited by the number of genes in a transcriptome that are assigned
140 functional terms. Because our custom annotation is limited in terms of scope and functional
141 category, we applied gene ontology (GO) term GSEA (GO-GSEA) analysis based on eggNOG
142 mapper orthological assignments [37]. GO-GSEA provided corroborative evidence that anti-
143 microbial and signaling responses were enriched at 1 and 3 days following RVFV exposure (Fig
144 2B, S2 Fig). By 7 dpf, GTPase signaling and overall regulation of signaling processes were
145 significantly enriched in RVFV exposed midguts compared to BF controls at 7dpf (Fig 2B, S2
146 Table). Lastly, constituents of the smoothened signaling pathway were depleted at 7 dpf but

147 unaffected upon bloodfeeding alone. Smoothened is a signaling pathway associated with the
148 Hedgehog/Gli signaling pathway, which is responsible for maintenance of cell polarity and tissue
149 development[38]. To further support the role of the smoothened signaling pathway, the
150 *Drosophila melanogaster* Ci/Gli consensus (GACCACCCA) was searched against the
151 promoters of the *Ae. aegypti* genome. Overrepresentation analysis of 3221 unique genes
152 across the genome with Ci/Gli promoters indicated that negative regulation of chromatin and
153 epigenetic regulation as well as negative regulation of DNA-templated transcription were major
154 processes controlled by this promoter(S3 Fig).

155

156

157

158 **Figure 2. Differential gene expression profiles at 1, 3 and 7 days post-treatment.**
159 A. Heatmap of bulk RNA-Seq data pools of 20 midguts per timepoint were ranked by the top
160 100 genes of the RVFV treatment group on the indicated dpf. Columns group individual
161 biological replicate z-scores of RPKM values for RVFV vs. BF by treatment group (RVFV, BF,
162 SF), then by timepoint. Number of replicates ranged from 2 to 4. B. GO-GSEA dotplot of RNA-
163 Seq differential expression categories for 1, 3 and 7 days post-treatment BF (bloodfed vs sugar-
164 fed) and RVFV (RVFV-exposed vs BF). GeneRatio refers to the proportion of the gene set of
165 interest divided by the total number of genes. Highlighted biological processes are noted in red
166 font. Numbers below indicate DEGs that were enriched (red triangle) or depleted (blue triangle).

167

168 Gene expression upon a noninfectious bloodmeal

169 To differentiate the effects of virus exposure from those of bloodfeeding alone, additional
170 experiments were performed to reveal effects on differential gene expression and histone
171 modifications. By providing proteinaceous nutrients critical for egg-laying, bloodfeeding is crucial
172 for reproduction. Because arbovirus infection of mosquitoes intrinsically requires a bloodfeeding
173 event, and it is therefore intricately tied to vector competence, we hypothesized that
174 bloodfeeding alone modulates midgut gene expression to favor mosquito permissiveness to
175 virus infection [32]. Comparison of blood-fed vs sugar-fed (BF v SF) mosquito midguts at 1 day
176 post-feeding (dpf) revealed 4480 DEGs (FDR, <0.10, Fig 2, S1 and S4 Figs, S2 Table). The
177 expression of digestive enzymes is well documented[39], cellular processes with the lowest
178 adjusted p values (padj) at each timepoint are highlighted here. Multiple RNA processing and
179 cellular biogenesis pathways were modulated 1 dpf. By 3 dpf, the bloodmeal was completely
180 digested; nevertheless mitochondrial processes remained elevated (Fig 2B). By 7 dpf,
181 processes affecting chromosome organization and cell cycle progression were modulated
182 compared to sugar-fed controls (S4 Fig).

183

184 Altered H3K27ac profiles in RVFV v BF

185 Next, to determine whether gene expression changes associated with bloodfeeding and RVFV
186 exposure were tied to H3K27ac and H3K9me3 modifications, we performed CUT&RUN on
187 midguts following a bloodmeal and at 1, 3, 7 dpf to RVFV MP12 (S4 and S5 Tables). RVFV
188 exposure led to incremental changes to global H3K27ac patterns over time that were lower than
189 that of BF at 1 dpf and gradually increased over the course of infection (Fig 3A, S5 Fig). By 7
190 dpf, RVFV-exposed midguts showed slightly higher levels of global acetylation patterns than BF
191 controls (Fig 3A). Upon analysis of statistically significant differences, a striking pattern
192 emerged. There were 31 significantly different H3K27ac peaks proximal to transcription start

193 sites (TSS) at 1 dpf (Fig 3B). Of these, 24/30 (80%) peaks were depleted in RVFV-exposed and
194 just 6 peaks showed higher levels than BF controls. Though the number of altered H3K27ac
195 peaks were much greater following a bloodmeal alone, the overall proportion of
196 depleted/enriched peaks were similar (74% peaks depleted).

197 By 3 dpf, an overall increase in H3K27ac enrichment occurred for both treatment groups (red
198 bars, Fig 3B). Nevertheless, the proportion of significantly enriched H3K27ac peaks was
199 reduced in RVFV-exposed (41%) compared to BF v SF treatment group(23% depleted, Fig 3B,
200 S5 Table). This trend was even more dramatic at 7 dpf, wherein acetylation patterns in RVFV-
201 exposed mosquitoes showed a marked reduction in acetylation sites compared to BF controls.
202 In particular, 705/802 (88%) significant peaks were depleted in RVFV exposed midguts
203 compared to just 29% in the BF v SF group (Fisher's exact test, $p<0.0001$, Fig 3B, S5 Table).
204 Genes of interest proximal to TSS in RVFV-treated samples showed trends in H3K27ac
205 occupancy over time that are expected to affect cell morphogenesis at 1 dpf, regulation of
206 transcriptional processes at 3 dpf and membrane transport by 7 dpf (S6 Fig). We currently
207 cannot distinguish between the possibilities that overall dysregulation is occurring or whether
208 these effects are due to viral hijacking.

209

210 **Figure 3. Midgut histone modification profiles.** A. Representative H3K27ac peak heatmaps
211 of aligned reads at 1, 3 and 7 days post-treatment show global trends within 2 kB of TSS (x
212 axis). Reads were standardized to reads per genome coverage (RPGC). Y-axis indicates RPGC
213 of input-subtracted read alignments. B. Proportion of DiffBind peaks within 2 kB of TSS (FDR <=
214 0.10) for H3K27ac, (red = enriched peaks compared to control, blue = depleted peaks
215 compared to control) and H3K9me3 (orange = enriched, maroon = depleted). Total numbers of
216 DiffBind peaks within 2 kB of TSS listed to the right of the bars.

217

218 Bloodfeeding alone was associated with changes to H3K27ac peak patterns that varied over the
219 timecourse. Interestingly, global distributions of H3K27ac patterns increased upon bloodfeeding
220 compared to SF but waned by 3 dpf (Fig 3A). Of 4073 quantitatively differential BFvSF
221 CUT&RUN peaks at 1 dpf, 3271 were within 2 kB of DEG TSS (S4 Table, Fig3B). Of those, just
222 24% of peaks were quantitatively enriched in BF compared to SF controls. At 3 dpf, the overall
223 numbers of differential peaks were lower, however the proportion of those that were enriched
224 increased to 0.77. By 7 dpf, the sugar-fed group shows markedly higher levels of acetylation
225 than either treatment group, which may be an indicator of aging in the absence of a bloodmeal
226 (Fig 3A). GO-GSEA of genes proximal to TSS showed categories that were consistent with
227 those of RNA-Seq data (S4 Fig), with genes affecting RNA metabolism showing modulation of
228 H3K27ac marks at 1 dpf. These altered genomic regions supported changes to regulation of
229 metabolic processes by 3 dpf. Finally, by 7 dpf, genes responsible for controlling chromosomal
230 reorganization were identified proximal to H3K27ac sites.

231 Gene set over-representation analysis (GSORA) of gene functional categories for genes
232 proximal to H3K27ac marks (MACS2 peaks) showed changes over time in blood-fed vs
233 sugarfed controls(S7 Fig). In particular, at 1 dpf, peaks proximal to genes associated with
234 chromosomal organization and histone modifications were altered in the BF treatment group, a
235 pattern that shifted to catabolic and amide biosynthetic processes by 3 dpf (S7 Fig). These
236 associations continued over time. In contrast, at 7 dpf, both SF and BF samples showed
237 H3K27ac marks proximal to genes involved in several intracellular transport categories,
238 including vesicle-mediated, amide and peptide transport (S7 Fig).

239

240

RVFV DEGs with altered H3K27ac patterns

Correlation of DEGs with H3K27ac marks varied across the timecourse. In RVFV-exposed at 1 dpf, no differentially expressed genes had changes to proximal H3K27ac marks. However, at 3 dpf, 9 of 2023 DEGs did. By 7 dpf, there were 7/102 DEGs with depleted promoter-proximal acetylation patterns (S7 Table), 5 of which had enriched RNA levels, consistent with active gene expression. Of these 5 genes, 2 code for proteins that facilitate protein-protein interactions on cellular membranes, including AAEL005849 (synaptic vesicle protein) and AAEL019495 (pleckstrin/PDZ domain). Predicted gene function, coupled with transcript enrichment support the idea that these genes are proviral in supporting virus assembly or intracellular transport. A third gene, AAEL021746 (LysM-TLDc domain), which is predicted to regulate oxidative stress, showed enrichment of transcripts and depletion of H3K27ac marks[40]. The 2 genes with transcript depletion coupled with depletion of H3K27ac marks in RVFV-exposed midguts are predicted to have anti-viral function. One gene was a cytochrome P450 (CYP307A1, AAEL009762) and the second was a leucine-rich repeat (AAEL023746), which could be a novel pattern-recognition receptor.

Post-bloodmeal gene expression changes coincide with histone modifications

A key goal of this study was to identify associations between gene expression changes and histone marks. One day following a noninfectious bloodmeal, about one fourth of all DEGs (1052/4480) showed proximal H3K27ac marks (S5 Table). There were 512 depleted DEGs among those that had altered peaks. Of those, 383/512 showed corroborative depletion of H3K27ac marks. However, for the enriched peaks, just 84/540 enriched DEGs showed the

264 expected pattern of peak enrichment. S8 Fig shows the pattern of DEGs to promoter-proximal
265 DiffBind peaks across all 3 chromosomes. This indicates that regulatory features cannot be
266 explained by H3K27ac enrichment alone. At later timepoints following a bloodmeal alone, even
267 fewer enriched DEGs showed corroborative H3K27ac enrichment, 6/676 and 11/140 at 3 and 7
268 dpf, respectively.

269

270 Association between H3K9me3 peak patterns and RVFV-
271 associated de-repression at 3 dpf

272 H3K9me3 marks may be associated with poised enhancers or transcriptional repression,
273 depending on adjacent chromatin signatures[41, 42]. Our initial hypothesis was that H3K9me3
274 could underpin viral associated gene repression. Analysis of differentially bound H3K9me3
275 peaks by DiffBind showed depletion of peaks following RVFV exposure at 1 and 3 dpf (Fig 3B,
276 maroon bar, S6 Table, S5 and S9 Figs), which was consistent with transcriptional de-
277 repression. No DEGs overlapped with H3K9me3 peaks at 1 dpf. By 3 dpf, however, 109 DEGs
278 showed peaks within 2 kB of TSS (S6 Table). Specifically, of 754 differentially bound peaks in
279 the 3 dpf RVFV vs BF group, 109 DEGs showed proximal H3K9me3 peaks, 115 of 119 of these
280 peaks were depleted. Peak depletion was corroborated by the observation that 60 of 109 DEGs
281 were enriched (S2 Table). GO-GSEA analysis showed that processes affecting behavior and
282 general metabolic processes were proximal to these marks. Therefore, instead of controlling
283 part of viral repression of gene expression, as expected, our data was consistent with the idea
284 that depletion of H3K9me3 peaks at 3 dpf was a correlate of gene de-repression.

285

By 7 dpf, just one DEG in the RVFV-exposed group, AAEL021746, showed significant depletion of H3K9me3 peaks. Overall, alterations in H3K9me3 marks were not associated with as many significant genes of interest as H3K27ac marks were, except for AAEL021746.

Enhancers

Enhancers are long-range regulatory elements that activate or repress gene expression. H3K27ac marks are most often associated with enhancer activation of gene expression, whereas H3K9me3 enhancers are typically associated with transcriptionally repressed regions[42-44]. To explore potential involvement of enhancers, we interrogated our datasets for the presence of H3K27ac or H3K9me3 marks that were 50,000 to 200,000 nts away from TSSs. H3K27ac enhancers were associated with bloodfeeding at 1, 3 and 7 dpf (S10 Fig). At 1 dpf, the genes with these putative enhancer elements coded for RNA processing and metabolic changes (S10A Fig). In contrast, H3K27ac enhancers were enriched upon RVFV exposure only at 3 dpf.

Putative H3K9me3 enhancers were generally depleted upon bloodfeeding at 1 and 3 dpf (S10 FigB, maroon bar), which would be consistent with large-scale changes in metabolic needs, necessitating broad scale re-structuring of chromatin concomitant with gene expression changes. For RVFV exposed samples, enhancers were enriched at 1 and 7 dpf, which supports our hypothesis of virus-induced transcriptional repression. However, this interpretation is complicated by the lack of altered peaks at 3 dpf.

307 # Discussion

308 Global changes in H3K27ac marks occurred in a layered fashion in *Ae. aegypti* midguts upon
309 receiving a non-infectious bloodmeal or concomitant RVFV MP12 exposure. At 1 dpf, BF v SF
310 and RVFV v BF H3K27Ac peak profiles showed similarity in the overall numbers of peaks (Fig
311 3B). Blood-feeding alone led to an increase in enriched acetylation marks by 3 dpf, but those
312 levels were reduced in RVFV-exposed midguts. By 7 dpf, RVFV exposed midguts showed
313 significant depletion of H3K27ac marks relative to BF controls(Fig 3B). These results were
314 corroborated in the RNA-Seq data, with 70% of DEGs being depleted in the RVFV-exposed
315 group compared to BF controls at 7 dpf (Fig 2B). Moreover, the mean and median peak widths
316 for peaks enriched in BF were significantly larger than those enriched for RVFV-exposed pools.
317 Summary statistics of peak data indicate that RVFV-exposed pools had more peaks at promoter
318 regions, whereas peaks in the BF treatment group had higher representation in gene bodies.
319 These results are consistent with the idea that competitive regulatory processes are stimulated
320 upon virus exposure, with the host activating gene expression to enhance anti-viral defense,
321 while RVFV nonstructural protein on the S segment (NSs) or other viral protein(s) selectively
322 alters gene expression to enhance infection [45, 46]. The patterns changed over time, indicating
323 that elapsed time was required for significant histone modifications to occur. Alternatively, the
324 increasing level of signal over time could be illustrative of a small percentage of infected cells at
325 1 dpf that expanded to a higher percentage over the course of infection[47].
326
327 The study of transcriptional regulation *in vivo* is critical, because histone modification patterns
328 are not synonymous across cell culture and mosquito tissues [48]. Midguts are comprised of
329 mixed cell populations with differing competency for virus infection[47]. The results captured
330 here do not distinguish between different cell types or infection status. In addition, midgut pools
331 were used for each replicate sample, thus reducing the high level of variability expected for

individual mosquitoes[4]. Therefore, the patterns seen here represent overall trends associated with viral exposure.

RVFV-responsive host gene expression changes for a variety of functional categories occurred over time. For example, stimulation of cellular differentiation processes at 1 dpf were consistent with metabolic changes that might be required to support production of viral replication complexes(Fig 2C) [47]. These were coupled with repression of transcripts coding for dicarboxylic acid and glutamine metabolic processes, which could affect cellular signaling[49]. By 3 dpf, cellular processes specific to cell polarization processes were modulated (detection of light stimulus, phototransduction), as well as transcripts that control mitochondrial gene expression/translation (S3 Fig). By 7 dpf, signal transduction processes were repressed upon RVFV-exposure but not upon blood-feeding alone. In particular, components of the smoothened signaling pathway were depleted in the RVFV-exposed group(S4 Table, Fig3B). Smoothened is a frizzled class G-protein coupled receptor that acts in the hedgehog/Gli pathway to regulate cell polarity[38, 50]. Multiple lines of evidence indicate that arboviruses preferentially replicate in polarized cell types[51-53]. RVFV enters polarized mammalian cells more efficiently through the apical surface, and viral particles mature near basolateral membranes[54]. The smoothened pathway has antiviral characteristics in mammalian neuronal cells, therefore repression would likely favor viral propagation [55]. Though genes with C/Gli promoters were present across the sample sets (S8 Table), the gene set was not detected by GSEA until 7 dpf. We speculate that repression of transcripts in the smoothened pathway is proviral in mosquitoes; nevertheless, this will have to be explored further to determine the full extent of these interactions.

Interestingly, one DEG, AAEL021746 (LysM-TLDc domain), which was slightly enriched in RVFV exposed midguts at 7 dpf, showed significant depletion of both H3K9me3 and H3K27ac peaks. This gene also has a C/Gli promoter motif (S8 Table). LysM-TLDc containing proteins,

358 e.g. human NCOA7 (Nuclear receptor coactivator 7), have been shown to interact with vacuolar-
359 ATPase, which promotes endoplasmic vesicle acidification to impair infection of influenza A
360 virus, human immunodeficiency virus and SARS-CoV[56-58]. This evidence suggests that
361 LysM-TLDc domain containing proteins, such as AAEL021746, have anti-viral activity.

362 We demonstrated enrichment of immune response transcripts at 1 and 3 dpf, which were above
363 and beyond what was induced by a noninfectious bloodmeal. RVFV-responsive genes of
364 interest included defensin (AAEL003832, AAEL003857), cecropin (AAEL029046,
365 AAEL029047), as well as transcriptional regulators that control immune transcriptional
366 responses. However, by 7 dpf, immune response transcripts, e.g., pattern recognition proteins
367 (AAEL001414, AAEL001420, AAEL010125, AAEL023746, AAEL024406) were depleted relative
368 to BF controls.

369 Overall, these results are consistent with a gradual increase in the efficacy of viral repression of
370 host gene expression over time. There are multiple examples of arboviral proteins that enter the
371 nucleus to interact with transcriptional machinery[46, 59]. Bunyamwera (*Orthobunyavirus*
372 *bunyamweraense)* nonstructural protein NSs interacts directly with *Mediator 8*[46]; the mediator
373 complex ties RNA polymerase II to a host of transcription factors. In humans, the RVFV
374 nonstructural NSs enters the nucleus to transcriptionally modulate beta catenin expression[45,
375 60]. NSs protein also suppresses host transcription, including of interferon beta, and degrades
376 host protein kinase R (PKR, EIFAK2); these actions collectively facilitate viral replication as host
377 cell machinery is co-opted and anti-viral responses are shut down[3, 61]. Even though the
378 current study utilized an attenuated strain of RVFV, NSs remains fully functional[62]. In another
379 study, *Ae. aegypti* infected with a deletion mutant strain of RVFV lacking NSs showed
380 significantly reduced virus dissemination rates, indicating that this protein is playing some role in
381 mosquito infection in addition to the roles described during vertebrate infection[24]. Therefore,

382 progressive modulation of immune gene transcription and cell cycle processes in RVFV-infected
383 mosquitoes may be related to NSs activity as an infection establishes in the mosquito midgut.
384

385 A previous report from Zhu et. al. showed that bloodfeeding alone prepared mosquitoes
386 metabolically to favor arbovirus infection[32]. In the current study, over one quarter of all DEGs
387 in the BF group at 1 dpf showed evidence of proximal H3K27ac marks. In addition, exposure to
388 a noninfectious bloodmeal resulted in enrichment of immune response genes, likely a
389 preventative measure to protect against potential pathogens present in the bloodmeal (S3
390 Table) [63]. Because H2K27ac promotes chromatin accessibility for gene expression, this result
391 supports the hypothesis that bloodfeeding alone sets up favorable regulatory conditions that
392 would favor viral hijacking. BF histone modification patterns were dramatically different than SF
393 as early as 1 dpf, eased by 3 dpf and, then by 7 dpf, mosquitoes that had not received a
394 bloodmeal showed substantially higher H3K27ac levels than the other treatment groups,
395 consistent with a possible role in aging. Genes proximal to H3K27ac marks in SF mosquitoes
396 did not change much over the course of time in terms of functional category type (S7 Fig).
397

398 A more competent vector might have less of a pronounced immune response at these early
399 timepoints. *Ae. aegypti* has an intermediate level of competency for RVFV infection and
400 transmission. Competence is much less than that of *Cx tarsalis* and higher than that of *Cx*
401 *pipiens quinquefasciatus*[23, 64]. GO-GSEA analysis showed that defense processes were
402 enriched at 1 and 3 dpf but repressed by 7 dpf. These observations were consistent with active
403 immune response gene expression early in infection as part of overall intrinsic immune
404 responses, which are key determinants of mosquito vector competence[65]. We would expect
405 that a more susceptible mosquito species would show immune response repression earlier in

406 the course of infection. However, further experiments are needed to sort out chromatin
407 modulation across susceptible and resistant phenotypes.

408

409 Tri-methylation of histone 3 (H3K9me3) is associated with gene silencing. Due to the expected
410 selective reduction in gene expression upon viral infection[45], we initially hypothesized that
411 H3K9me3 marks might be enhanced during virus infection but found that instead, the global
412 changes to H3K9me3 marks were much less dramatic than those found for
413 H3K27ac. Nevertheless, significant depletion of H3K9me3 marks was observed in the 3 dpf
414 RVFV vs BF group, which is consistent with derepression of gene expression. It is currently
415 unclear whether this marked derepression at a time when viral replication complexes are active
416 is part of viral hijacking or the host response.

417 Overall, these results provide support for the idea that histone modifications are part of the
418 overall mosquito response to arbovirus infection. However, the extent to which specific changes
419 are manipulated by viral proteins or a part of the host defense response must be determined by
420 further experimentation.

421

422 Conclusion

423 H3K27ac marks are significantly altered upon exposure to RVFV MP12, with a subset of DEGs
424 that had significant changes indicative of active gene expression. However, competing
425 processes for control of H3K27ac levels seem to be at play. Future efforts will continue to
426 explore the epigenetic landscape layers in arbovirus exposed mosquitoes to identify the major
427 players responsible for virus-induced transcriptional repression and whether these changes are

428 consistent across arbovirus systems.

429

430 Materials and Methods

431 Mosquito and virus experiments

432 The Poza Rica strain of *Ae. aegypti* was colonized in 2012, originating from the state of
433 Veracruz, Mexico[66]. Mosquito colonies were maintained at 28 °C on a 12:12 light:dark cycle;
434 adults were fed water and sucrose (sugar cubes or raisins) *ad libitum*. Larvae were reared on
435 TetraMin fish food (Spectrum Brands Pet, Blacksburg, VA, USA) ground in a coffee grinder.
436 Mosquitoes (3–7 days old) were starved for food and water for 24 hours prior to feeding, then
437 orally exposed to RVFV MP-12 or conditioned cell culture media mixed 1:1 with defibrinated
438 sheep blood, as described in Campbell et al.[23]. A high passage strain of MP12 (passage
439 unknown, local lab passage 1), which was a gift from the US Department of Agriculture, was
440 used for these experiments. In brief, freshly grown MP-12 RVFV was grown in Vero cells at a
441 multiplicity of infection of 0.01 for 3 days and then mixed 1:1 in defibrinated calf blood (Colorado
442 Serum Company, Denver, CO, USA), with 1 mM ATP as phagostimulant and orally provided to
443 adult mosquitoes in water-jacketed feeders set to 37°C. Viral bloodmeal titers were at 6.9–7.8
444 log10 plaque-forming units (PFU) per ml. As a control, a separate group of age-matched
445 mosquitoes were held for the indicated period. Three replicates of each experiment were
446 performed.

447 Plaque assays were done using methods described previously[23]. Midgut infection rates were
448 determined as follows. Individual mosquito carcasses were placed in 250 µl mosquito diluent
449 (DMEM, 20% heat-inactivated FBS, 50 µg/ml Pen-Strep, 50 µg/ml gentamicin, and 2.5 µg/ml
450 amphotericin B) following removal of midguts for CUT&RUN and stored at -80°C. Samples were

451 homogenized on a Qiagen Tissuelyzer (Qiagen) at 30 beats per second frequency for 30
452 seconds. Homogenates were pelleted for 3 minutes at 21,000 x g, then 50 µl homogenate was
453 placed into one well of a 12 well plate and assayed in duplicate. At 3 days post-infection, wells
454 were assessed for cytopathic effects.

455

456 CUT&RUN

457 Our approach followed that of Skene, et al.[30] with modifications. Specifically, pools of 20
458 midguts from blood-fed and RVFV MP12-fed *Aedes aegypti* were dissected 1, 3 and 7 days
459 post feed or from sugar-fed controls. Midguts were placed into 200 µL of 1x Schneider's
460 Drosophila Media (Gibco #21720024). Following completion of dissections for all samples, 300
461 µL of formaldehyde fixation solution was added to each tube for a final concentration of 0.1%
462 (using 16% methanol-free formaldehyde (Cell Signaling # 12606) in phosphate buffered saline
463 (PBS) with 1x protease inhibitor cocktail (PIC, cOmplete™ Protease Inhibitor Cocktail, #
464 11697498001). After a 10-minute incubation at room temperature, 50 µL of 10x Glycine (Cell
465 Signaling #7005) was added to stop the reactions and samples were incubated for another 5
466 minutes at room temperature (RT). Samples were centrifuged for 5 minutes at 2000xg 4°C then
467 washed with 500 µL PIC/PBS. At all steps, tubes were flicked to mix solutions rather than
468 pipetting to prevent loss of midguts. Midguts were resuspended in 1 ml Wash buffer (200mM
469 HEPES pH 7.5, 1.5 M NaCl, 0.5 mM spermidine, 1x PIC), then centrifuged for 3 min at 2,000 xg
470 at RT. Each reaction was resuspended in 100 µL 1x Wash buffer. Ten µL per sample of
471 concanavalin A beads (Fisher # NC1831103) were activated using the methods of Skene, et
472 al.[30]. Then the beads were added to the sample and incubated 5 minutes at RT. Each sample
473 tube was placed on a magnetic stand (ThermoFisher 12321D). Once the solution cleared, the
474 liquid was removed and replaced with 100 µL Digitonin solution (200mM HEPES pH 7.5, 1.5M

475 NaCl, 20mM spermidine, 1x PIC, 0.1% digitonin) with 2mM EDTA and the appropriate antibody.
476 The antibodies used in this study were 2 µg per reaction anti-H3K27ac Ab (Abcam, ab4729), or
477 1 µg per reaction anti-H3K9me3 Ab (Abcam, ab8898) and Rabbit (DA1E) mAb IgG XP® Isotype
478 Control (Cell Signaling #66362) as a negative control. Samples were incubated overnight at 4°C
479 on a rotator. Then the samples were put on the magnetic stand. Once the solution was clear,
480 the samples were washed with 1 ml Digitonin buffer and put back on the stand. Upon removing
481 the buffer, 50 µL solution containing 1.5 µL protein A/G- micrococcal nuclease (pAG/MNase,
482 Epicypher, #15-1116) in Digitonin buffer was added per sample and mixed gently by flicking the
483 tube. Samples were incubated at 4°C for 1 hour. The samples were then washed twice as
484 before in 1 ml Digitonin buffer per sample. Samples were resuspended in 150 µL Digitonin
485 buffer, placed on ice for 5 minutes, then activated by adding 3 µL 100 mM cold Calcium
486 Chloride to each tube. Samples were incubated at 4°C for 30 minutes. Reactions were stopped
487 by the addition of 150 µL Stop buffer (0.17 M NaCl, 10mM EDTA, 2mM EGTA, 0.1 mg/ml
488 glycogen, 0.1% Digitonin, 8.3 mg/ml RNAse A). Samples were the centrifuged at 3 min at
489 16,000 xg for 2 minutes. Supernatants were transferred to new tubes containing 3 µL 10%
490 sodium dodecyl sulfate and 2 µl Proteinase K (20 mg/ml). Samples were then incubated at 65°C
491 for 2 hr, then transferred to low bind tubes. DNA fragments were purified using Qiagen PCR
492 purification kits.

493 Input sample preparation

494 Input samples were processed in parallel with the other samples through the first wash steps.
495 Total DNA was extracted using a salt extraction method and resuspended in 100µl water [67].
496 Following extraction, samples were placed in a 0.65 mL Diagenode tube and sonicated in a
497 Diagenode Bioruptor Pico (Diagenode) for 20 cycles of 30 seconds on, 30 seconds off.
498 Fragment sizes of ~200 bp were subsequently validated using an HS D1000 chip with an
499 Agilent 4150 tapestation (Agilent).

500

501 ## Sequencing

502 Three biological replicates were sequenced per sample group. Briefly, standard library
503 preparation methods made use of the NEBNext® Ultra™ II DNA Library Prep Kit for Illumina
504 (E7103L) following manufacturer's directions with 1 ng DNA per library prep and ~13 PCR
505 cycles for the amplification step. Library quality was confirmed using high sensitivity DNA
506 reagents (Q33231) on the Qubit 2 (Qubit) and Agilent tapestation 4150 (Agilent). Sequencing
507 was performed on an Illumina NovaSeq (Azenta.com) with read depths indicated in S2 Table.
508 Libraries with less than 55 nt inserts were removed from analysis (S2 Table).
509

510 ## Analysis

511 All scripts utilized for the analysis of this data can be found on GitHub
512 (https://github.com/CRosenbergCode/Aedes_aegypti_Midgut_CUT-RUN), Sequencing reads
513 were trimmed and filtered using Fastp version 0.23.4[68]. Duplicate reads were removed for
514 ChIP-seq reads but retained for RNA-seq analysis[69]. These trimmed and filtered reads were
515 aligned to an index prepared from the VectorBase-68_AaegyptiLVP_AGWG_Genome.fasta
516 using HISAT2 version 2.2.1[70, 71]. Only paired reads which aligned concordantly were
517 retained. Data regarding alignment rates and quality parameters per sample can be found in
518 Supplemental Tables 1-3. Peak calling was performed on merged alignments using MACS2
519 macs2 2.2.9.1 using --keep dups all, qvalue 0.05 against VectorBase-
520 68_AaegyptiLVP_AGWG_Genome.fasta [71, 72]. All samples were standardized using the
521 corresponding input sample.
522 Bigwig files were created using Deeptools bamCoverage with a bin size of 10 bases and
523 normalized using reads per genome coverage (RPGC)[73]. They were then compared against

524 their corresponding inputs using Deeptools bigwigCompare, with a bin size of 10 bases and --
525 operation subtract, thus generating bigwigs that use direct subtraction as opposed to fold
526 change. Peak heatmaps and read density maps were made using deepTools functions
527 “computeMatrix”, and “plotHeatmap”. computeMatrix was run with the “make_matrices.sh” script
528 using VectorBase-68_AaegyptiLVP_AGWG_Genome.bed (No MIT, long-noncoding RNAs or
529 pseudogenes) as reference.
530 Differential binding analysis was performed using Diffbind version 3.12.0 with the edgeR option
531 [74] in R version 4.3.2[75] using a false discovery rate(FDR) threshold of $p<0.10$. A custom
532 script was created to determine the proximity of DiffBind peaks to genes or other features of
533 interest in the *Ae. aegypti* genome (S4 and S5 Tables).

534

535 RNA Sequencing and analysis

536 Three to 4 biological replicates were sequenced per sample group. Bulk RNA-Seq libraries were
537 prepared from 200 ng total RNA, using polyA+ purification (NEBNext® Poly(A) mRNA Magnetic
538 Isolation Module) prior to library prep with the NEBNext® Ultra™ II Directional RNA Library Prep
539 Kit for Illumina. Sequencing was performed on an Illumina NovaSeq (Azenta.com) with read
540 depths indicated in S1 Table.

541 For RNA-seq alignment, a reference transcriptome was created using VectorBase-
542 68_AaegyptiLVP_AGWG_AnnotatedTranscripts.fasta [71] using HISAT2 (2.2.1)[70], then
543 alignment was performed using standard parameters. Gene-level aggregation was performed
544 using HTseq-count (2.0.5). Differential expression analysis was performed using DEseq2
545 (1.48.0).

546

547

548 ## Gene Set Enrichment analysis

549 GO-GSEA libraries were built using AnnotationForge version 2.13 in R. Genome-wide
550 annotation was performed using Entrez gene identifiers[39]. The fast gene set enrichment
551 analysis algorithm R implemented by the fgsea R package (version 1.28.0) [76] was used for
552 GO-GSEA analysis[77]. GO terms were obtained using EggNog Mapper 2.1.12, limiting the
553 orthology search to Diptera only[37]. Custom annotations were utilized to define broader
554 functional categories as described in Campbell et al 2019 [33]. For both GSEA (ranked
555 nonparametric analysis) and ORA (simple arithmetical calculation that does not involve ranking),
556 a minimum size of 15 and a maximum size of 500 were required for a GO annotation to be
557 included in analysis. Ranking was based on the -log10(p-value). In all cases, ordering was
558 decided arbitrarily in case of ties. GO-GSEA of RNA-seq differential binding was based on
559 DESeq2 results. GO-GSEA of ChIP-seq differential binding was based on Diffbind results. In
560 cases of multiple peaks corresponding to the same gene, only the peak with the highest p-value
561 was retained. For ORA, duplicate peaks for the same gene were removed to ensure each gene
562 only occurred once. For analysis of promoters, only peaks within 2000 bp of the TSS were
563 included for the analysis. For analysis of enhancers, only peaks between 50,000 and 200,000
564 bp away from a TSS that were annotated as distal using ChIPSeeker were included for the
565 analysis[78, 79]. The custom annotation was manually compiled based on Campbell et al 2019,
566 which relied on VectorBase orthological assignments[33, 71].The custom OrgDB database and
567 GMT files used are provided on the github for this manuscript. Visualization of gene enrichment
568 utilized enrichplot version 1.28 [80] and ClusterProfiler version 4.15[81].

569 ## Motif Enrichment analysis

570 Enrichment analysis was performed using HOMER (Hypergeometric Optimization of Motif
571 EnRichment) version 5.1 with a custom genome created using VectorBase-
572 68_AaegyptiLVP_AGWG annotations[82]. An offset of 2000 base pairs upstream and 200 base
573 pairs downstream of the transcription start site were used and a random selection of promoter
574 regions was used as the background. For searching known motifs such as CI/GLI binding sites,
575 the consensus sequence (GACCACCCA) in *D. melanogaster* was used and a maximum of 1
576 mismatch was allowed. Genes from this study with these motifs are in S8 Table.

577

578

579 # Supporting Information

580 **S1 Table.** RNA-Seq raw reads with Q20/Q30 scores, insert sizes and alignment rates.

581 **S2 Table.** RNA-Seq DESeq2 analysis for all samples and timepoints.

582 **S3 Table.** Normalized Enrichment Score Table for RVFV v BF time course.

583 **S4 Table.** CUT&RUN-Seq raw reads with Q20/Q30 scores, insert sizes and alignment rates.

584 **S5 Table.** H3K27ac DiffBind output for genes within 2kB of TSS.

585 **S6 Table.** H3K9me3 DiffBind output for genes within 2kB of TSS.

586 **S7 Table.** RVFV v BF DEGs with proximal H3K27Ac peaks at the 7dpe

587 **S8 Table.** CI/GLI promoter regions identified using HOMER.

588

589 **S1 Fig. MA plots of RNA-Seq differential expression data**.

590 **S2 Fig. GO-GSEA of RVFV v BF RNA-Seq differential expression data.**

591 **S3 Fig. Over-representation analysis of all *Ae. aegypti* genes with Ci/Gli motif.**

592 **S4 Fig. GO-GSEA of BF vs SF RNA-Seq transcript differential expression data.**

S5 Fig. H3K27ac and H3K9me3 peak profiles. Top row: H3K27ac Input-subtracted peak heatmaps of aligned reads at 1, 3 and 7 days post-treatment show global trends within 2 kB of TSS (x axis). Y-axis indicates RPGC (reads per genome coverage) of input-subtracted read alignments. Notice the different Y-axis scales. Bottom row: H3K9me3 Input-subtracted peak heatmaps.

S6 Fig. RVFV vs BF datasets: GSEA of GOls proximal to H3K27Ac and H3K9me3 marks.

S7 Fig. GO categories for genes proximal to H3K27ac marks change over time. A. GO terms for genes within 2kB of TSS (MACS2 peak calls) displayed using over-representation analysis. X axis shows collection day (d1, d3, or d7), BF, bloodfed, SF, sugar-fed. Number in parentheses below the sample name indicates the number of macs2 peaks considered in the analysis. This is a qualitative analysis and does not indicate statistically significant differences between groups. B. Transition of GO terms over time in BF midguts. GO terms for genes within 2kB of TSS (DiffBind peak calls) displayed using over-representation analysis.

S8 Fig. BFvSF 1 dpf: Relationship of H3K27ac peaks and DEGs. Coordinates for DEG start sites (DEG Log2FC, right y-axis) were plotted alongside H3K27ac peak coordinated and fold-change values (Peak FC, left y-axis).

S9 Fig. H3K9me3 RVFV vs BF vs SF peak heatmaps. Input-subtracted H3K9me3 peak heatmaps of aligned reads at 1, 3 and 7 days post-treatment show global trends within 2 kB of TSS (x axis). Y-axis indicates RPGC (reads per genome coverage) of input-subtracted read alignments.

S10 Fig. Enhancers. A. GSEA functional groups of genes at the BF v SF 1 dpf timepoint that showed predicted H3K27ac peaks. B. Proportion of DiffBind peaks within 2 kB of TSS (FDR <= 0.10) for H3K27ac, (red = enriched, blue = depleted) and H3K9me3 (orange = enriched, maroon = depleted). Total numbers of DiffBind peaks within 2 kB of TSS listed to the right of the bars.

Acknowledgements

We thank the Swygert lab at Colorado State University for the use of their Bioruptor Pico instrument. RVFV MP-12 virus stock was kindly provided by the United States Department of Agriculture, Agricultural Research Service. Figures 1A and 1B were generated in BioRender (BioRender.com).

Informed Consent Statement: Not applicable.

Data Availability Statement: Raw data available upon request. All raw sequencing data has been uploaded to the NCBI Sequence Read archive under Bioprojects PRJNA1284329 and PRJNA1290393**.**

Conflicts of Interest

The authors declare no conflict of interest.

Funding

This project was funded by a Non-Assistance Cooperative Agreement 3022-32000-018-033-S to CLC from the USDA Agricultural Research Service, NIH-NIGMS R35GM124877 and NSF MCB CAREER 2143849 awards to EON.

Author Contributions

Conceptualization: C Campbell

Data curation: C Campbell, H Ogg

Formal analysis: Z Arhouma, C Campbell, H Ogg, Z Mikol

Funding acquisition: C Campbell, C Mire

Methodology: Z Arhouma, D King, H Ogg, Z Mikol

Validation: E Osborne Nishimura, D King, H Ogg, C Campbell

Project administration: C Campbell

Visualization: Z Mikol, H Ogg

Resources: R Kading, C Mire, C Campbell

Writing, original: C Campbell, H Ogg

Writing, review and editing: C Campbell, C Mire, R Kading, E Osborne Nishimura, D King

References

1. Weaver SC, Charlier C, Vasilakis N, and Lecuit M, Zika, Chikungunya, and Other Emerging Vector-Borne Viral Diseases. Annu Rev Med, 2018. **69**: p. 395-408. DOI: 10.1146/annurev-med-050715-105122.
2. Billecocq A, Spiegel M, Vialat P, Kohl A, Weber F, Bouloy M, et al., NSs protein of Rift Valley fever virus blocks interferon production by inhibiting host gene transcription. J Virol, 2004. **78**(18): p. 9798-806. DOI: 10.1128/JVI.78.18.9798-9806.2004.
3. Ikegami T, Narayanan K, Won S, Kamitani W, Peters CJ, and Makino S, Rift Valley fever virus NSs protein promotes post-transcriptional downregulation of protein kinase PKR and inhibits eIF2alpha phosphorylation. PLoS Pathog, 2009. **5**(2): p. e1000287. DOI: 10.1371/journal.ppat.1000287.
4. Smith CB, Hodges NF, Kading RC, and Campbell CL, Dishevelled Has Anti-Viral Activity in Rift Valley Fever Virus Infected Aedes aegypti. Viruses, 2023. **15**(11). DOI: 10.3390/v15112140.
5. Rehman UU, Ghafoor D, Ullah A, Ahmad R, and Hanif S, Epigenetics regulation during virus-host interaction and their effects on the virus and host cell. Microb Pathog, 2023. **182**: p. 106271. DOI: 10.1016/j.micpath.2023.106271.

672 6. Amarante AM, da Silva ICA, Carneiro VC, Vicentino ARR, Pinto MA, Higa LM, et
673 al., Zika virus infection drives epigenetic modulation of immunity by the histone
674 acetyltransferase CBP of Aedes aegypti. PLoS Negl Trop Dis, 2022. **16**(6): p.
675 e0010559. DOI: 10.1371/journal.pntd.0010559.
676 7. Caraballo GI, Rosales R, Viettri M, Castillo JM, Cruz R, Ding S, et al., The
677 Dengue Virus Nonstructural Protein 1 (NS1) Interacts with the Putative
678 Epigenetic Regulator DIDO1 to Promote Flavivirus Replication in Mosquito Cells.
679 J Virol, 2022. **96**(12): p. e0070422. DOI: 10.1128/jvi.00704-22.
680 8. Harrell T, Basak S, Sultana H, and Neelakanta G, Zika virus modulates arthropod
681 histone methylation for its survival in mosquito cells. PLoS One, 2025. **20**(2): p.
682 e0319290. DOI: 10.1371/journal.pone.0319290.
683 9. Zhou D, Wu Z, Park JG, Fiches GN, Li TW, Ma Q, et al., FACT subunit
684 SUPT16H associates with BRD4 and contributes to silencing of interferon
685 signaling. Nucleic Acids Res, 2022. **50**(15): p. 8700-8718. DOI:
686 10.1093/nar/gkac645.
687 10. Gaddelapati SC, Albishi NM, Dhandapani RK, and Palli SR, Juvenile hormone-
688 induced histone deacetylase 3 suppresses apoptosis to maintain larval midgut in
689 the yellow fever mosquito. Proc Natl Acad Sci U S A, 2022. **119**(11): p.
690 e2118871119. DOI: 10.1073/pnas.2118871119.
691 11. Carson WFt and Kunkel SL, Regulation of Cellular Immune Responses in Sepsis
692 by Histone Modifications. Adv Protein Chem Struct Biol, 2017. **106**: p. 191-225.
693 DOI: 10.1016/bs.apcsb.2016.08.004.
694 12. Daskalaki MG, Tsatsanis C, and Kampranis SC, Histone methylation and
695 acetylation in macrophages as a mechanism for regulation of inflammatory
696 responses. J Cell Physiol, 2018. **233**(9): p. 6495-6507. DOI: 10.1002/jcp.26497.
697 13. Chen CH, Zheng R, Tokheim C, Dong X, Fan J, Wan C, et al., Determinants of
698 transcription factor regulatory range. Nat Commun, 2020. **11**(1): p. 2472. DOI:
699 10.1038/s41467-020-16106-x.
700 14. Del Rosario RCH, Poschmann J, Lim C, Cheng CY, Kumar P, Riou C, et al.,
701 Histone acetylome-wide associations in immune cells from individuals with active
702 Mycobacterium tuberculosis infection. Nat Microbiol, 2022. **7**(2): p. 312-326. DOI:
703 10.1038/s41564-021-01049-w.
704 15. Padeken J, Methot SP, and Gasser SM, Establishment of H3K9-methylated
705 heterochromatin and its functions in tissue differentiation and maintenance. Nat
706 Rev Mol Cell Biol, 2022. **23**(9): p. 623-640. DOI: 10.1038/s41580-022-00483-w.
707 16. Li F, Nellaker C, Sabunciyan S, Yolken RH, Jones-Brando L, Johansson AS, et
708 al., Transcriptional derepression of the ERVWE1 locus following influenza A virus
709 infection. J Virol, 2014. **88**(8): p. 4328-37. DOI: 10.1128/JVI.03628-13.
710 17. Lezcano OM, Sanchez-Polo M, Ruiz JL, and Gomez-Diaz E, Chromatin Structure
711 and Function in Mosquitoes. Front Genet, 2020. **11**: p. 602949. DOI:
712 10.3389/fgene.2020.602949.
713 18. Gomez-Diaz E, Rivero A, Chandre F, and Corces VG, Insights into the
714 epigenomic landscape of the human malaria vector Anopheles gambiae. Front
715 Genet, 2014. **5**: p. 277. DOI: 10.3389/fgene.2014.00277.
716 19. Ruiz JL, Yerbanga RS, Lefevre T, Ouedraogo JB, Corces VG, and Gomez-Diaz
717 E, Chromatin changes in Anopheles gambiae induced by Plasmodium falciparum

718 infection. Epigenetics Chromatin, 2019. **12**(1): p. 5. DOI: 10.1186/s13072-018-
719 0250-9.
720 20. Behura SK, Sarro J, Li P, Mysore K, Severson DW, Emrich SJ, et al., High-
721 throughput cis-regulatory element discovery in the vector mosquito Aedes
722 aegypti. BMC Genomics, 2016. **17**: p. 341. DOI: 10.1186/s12864-016-2468-x.
723 21. Clark MHA, Warimwe GM, Di Nardo A, Lyons NA, and Gubbins S, Systematic
724 literature review of Rift Valley fever virus seroprevalence in livestock, wildlife and
725 humans in Africa from 1968 to 2016. PLoS Negl Trop Dis, 2018. **12**(7): p.
726 e0006627. DOI: 10.1371/journal.pntd.0006627.
727 22. Sang R, Kioko E, Lutomiah J, Warigia M, Ochieng C, O'Guinn M, et al., Rift
728 Valley fever virus epidemic in Kenya, 2006/2007: the entomologic investigations.
729 Am J Trop Med Hyg, 2010. **83**(2 Suppl): p. 28-37. DOI: 10.4269/ajtmh.2010.09-
730 0319.
731 23. Campbell CL, Snell TK, Bennett S, Wyckoff JH, 3rd, Heaslip D, Flatt J, et al.,
732 Safety study of Rift Valley Fever human vaccine candidate (DDVax) in
733 mosquitoes. Transbound Emerg Dis, 2022. **69**(5): p. 2621-2633. DOI:
734 10.1111/tbed.14415.
735 24. Crabtree MB, Kent Crockett RJ, Bird BH, Nichol ST, Erickson BR, Biggerstaff BJ,
736 et al., Infection and transmission of Rift Valley fever viruses lacking the NSs
737 and/or NSm genes in mosquitoes: potential role for NSm in mosquito infection.
738 PLoS Negl Trop Dis, 2012. **6**(5): p. e1639. DOI: 10.1371/journal.pntd.0001639.
739 25. Kading RC, Crabtree MB, Bird BH, Nichol ST, Erickson BR, Horiuchi K, et al.,
740 Deletion of the NSm virulence gene of Rift Valley fever virus inhibits virus
741 replication in and dissemination from the midgut of Aedes aegypti mosquitoes.
742 PLoS Negl Trop Dis, 2014. **8**(2): p. e2670. DOI: 10.1371/journal.pntd.0002670.
743 26. Laporta GZ, Potter AM, Oliveira JFA, Bourke BP, Pecor DB, and Linton YM,
744 Global Distribution of Aedes aegypti and Aedes albopictus in a Climate Change
745 Scenario of Regional Rivalry. Insects, 2023. **14**(1). DOI:
746 10.3390/insects14010049.
747 27. O'Dell N, Bolling BG, Dacko N, Carr JT, Hambrick B, Chaves LF, et al.,
748 Identifying environmental drivers of Aedes aegypti and Aedes albopictus
749 abundance in the Dallas-Fort Worth metroplex using Random Forest modeling. J
750 Med Entomol, 2025. DOI: 10.1093/jme/tjaf036.
751 28. Parker C, Ramirez D, and Connelly CR, State-wide survey of Aedes aegypti and
752 Aedes albopictus (Diptera: Culicidae) in Florida. J Vector Ecol, 2019. **44**(2): p.
753 210-215. DOI: 10.1111/jvec.12351.
754 29. Kaya-Okur HS, Janssens DH, Henikoff JG, Ahmad K, and Henikoff S, Efficient
755 low-cost chromatin profiling with CUT&Tag. Nat Protoc, 2020. **15**(10): p. 3264-
756 3283. DOI: 10.1038/s41596-020-0373-x.
757 30. Skene PJ, Henikoff JG, and Henikoff S, Targeted in situ genome-wide profiling
758 with high efficiency for low cell numbers. Nat Protoc, 2018. **13**(5): p. 1006-1019.
759 DOI: 10.1038/nprot.2018.015.
760 31. Yin H, Sweeney S, Raha D, Snyder M, and Lin H, A high-resolution whole-
761 genome map of key chromatin modifications in the adult *Drosophila*
762 *melanogaster.* PLoS Genet, 2011. **7**(12): p. e1002380. DOI:
763 10.1371/journal.pgen.1002380.

764 32. Zhu Y, Zhang R, Zhang B, Zhao T, Wang P, Liang G, et al., Blood meal
765 acquisition enhances arbovirus replication in mosquitoes through activation of the
766 GABAergic system. Nat Commun, 2017. **8**(1): p. 1262. DOI: 10.1038/s41467-
767 017-01244-6.
768 33. Campbell CL, Saavedra-Rodriguez K, Kubik TD, Lenhart A, Lozano-Fuentes S,
769 and Black WCI, Vgsc-interacting proteins are genetically associated with
770 pyrethroid resistance in *Aedes aegypti.* PLoS One, 2019. **14**(1): p. e0211497.
771 DOI: 10.1371/journal.pone.0211497.
772 34. Kubik TD, Snell TK, Saavedra-Rodriguez K, Wilusz J, Anderson JR, Lozano-
773 Fuentes S, et al., Aedes aegypti miRNA-33 modulates permethrin induced
774 toxicity by regulating VGSC transcripts. Sci Rep, 2021. **11**(1): p. 7301. DOI:
775 10.1038/s41598-021-86665-6.
776 35. Ma Y, Liang Y, Wang N, Cui L, Chen Z, Wu H, et al., Avian Flavivirus Infection of
777 Monocytes/Macrophages by Extensive Subversion of Host Antiviral Innate
778 Immune Responses. J Virol, 2019. **93**(22). DOI: 10.1128/JVI.00978-19.
779 36. Pott F, Postmus D, Brown RJP, Wyler E, Neumann E, Landthaler M, et al.,
780 Single-cell analysis of arthritogenic alphavirus-infected human synovial
781 fibroblasts links low abundance of viral RNA to induction of innate immunity and
782 arthralgia-associated gene expression. Emerg Microbes Infect, 2021. **10**(1): p.
783 2151-2168. DOI: 10.1080/22221751.2021.2000891.
784 37. Cantalapiedra CP, Hernandez-Plaza A, Letunic I, Bork P, and Huerta-Cepas J,
785 eggNOG-mapper v2: Functional Annotation, Orthology Assignments, and
786 Domain Prediction at the Metagenomic Scale. Mol Biol Evol, 2021. **38**(12): p.
787 5825-5829. DOI: 10.1093/molbev/msab293.
788 38. Nusslein-Volhard C and Wieschaus E, Mutations affecting segment number and
789 polarity in Drosophila. Nature, 1980. **287**(5785): p. 795-801. DOI:
790 10.1038/287795a0.
791 39. Hixson B, Bing XL, Yang X, Bonfini A, Nagy P, and Buchon N, A transcriptomic
792 atlas of Aedes aegypti reveals detailed functional organization of major body
793 parts and gut regional specializations in sugar-fed and blood-fed adult females.
794 Elife, 2022. **11**. DOI: 10.7554/eLife.76132.
795 40. Jaramillo-Gutierrez G, Molina-Cruz A, Kumar S, and Barillas-Mury C, The
796 Anopheles gambiae oxidation resistance 1 (OXR1) gene regulates expression of
797 enzymes that detoxify reactive oxygen species. PLoS One, 2010. **5**(6): p.
798 e11168. DOI: 10.1371/journal.pone.0011168.
799 41. Blackledge NP and Klose RJ, The molecular principles of gene regulation by
800 Polycomb repressive complexes. Nat Rev Mol Cell Biol, 2021. **22**(12): p. 815-
801 833. DOI: 10.1038/s41580-021-00398-y.
802 42. Zentner GE, Tesar PJ, and Scacheri PC, Epigenetic signatures distinguish
803 multiple classes of enhancers with distinct cellular functions. Genome Res, 2011.
804 **21**(8): p. 1273-83. DOI: 10.1101/gr.122382.111.
805 43. Creyghton MP, Cheng AW, Welstead GG, Kooistra T, Carey BW, Steine EJ, et
806 al., Histone H3K27ac separates active from poised enhancers and predicts
807 developmental state. Proc Natl Acad Sci U S A, 2010. **107**(50): p. 21931-6. DOI:
808 10.1073/pnas.1016071107.

809 44. Zhu Y, van Essen D, and Saccani S, Cell-type-specific control of enhancer
810 activity by H3K9 trimethylation. Mol Cell, 2012. **46**(4): p. 408-23. DOI:
811 10.1016/j.molcel.2012.05.011.
812 45. Le May N, Mansuroglu Z, Leger P, Josse T, Blot G, Billecocq A, et al., A SAP30
813 complex inhibits IFN-beta expression in Rift Valley fever virus infected cells.
814 PLoS Pathog, 2008. **4**(1): p. e13. DOI: 10.1371/journal.ppat.0040013.
815 46. Leonard VH, Kohl A, Hart TJ, and Elliott RM, Interaction of Bunyamwera
816 Orthobunyavirus NSs protein with mediator protein MED8: a mechanism for
817 inhibiting the interferon response. J Virol, 2006. **80**(19): p. 9667-75. DOI:
818 10.1128/JVI.00822-06.
819 47. Fitzmeyer EA, Dutt TS, Pinaud S, Graham B, Gallichotte EN, Hill JL, et al., A
820 single-cell atlas of the Culex tarsalis midgut during West Nile virus infection.
821 PLoS Pathog, 2025. **21**(1): p. e1012855. DOI: 10.1371/journal.ppat.1012855.
822 48. Qu J, Betting V, van Iterson R, Kwaschik FM, and van Rij RP, Chromatin profiling
823 identifies transcriptional readthrough as a conserved mechanism for piRNA
824 biogenesis in mosquitoes. Cell Rep, 2023. **42**(3): p. 112257. DOI:
825 10.1016/j.celrep.2023.112257.
826 49. Joo SS, Won TJ, Kim MJ, Hwang KW, and Lee DI, Interferon signal transduction
827 of biphenyl dimethyl dicarboxylate/amantadine and anti-HBV activity in HepG2
828 2.2.15. Arch Pharm Res, 2006. **29**(5): p. 405-11. DOI: 10.1007/BF02968591.
829 50. Hynes M, Ye W, Wang K, Stone D, Murone M, Sauvage F, et al., The seven-
830 transmembrane receptor smoothened cell-autonomously induces multiple ventral
831 cell types. Nat Neurosci, 2000. **3**(1): p. 41-6. DOI: 10.1038/71114.
832 51. Ahearn YP, Saredy JJ, and Bowers DF, The Alphavirus Sindbis Infects
833 Enteroendocrine Cells in the Midgut of Aedes aegypti. Viruses, 2020. **12**(8). DOI:
834 10.3390/v12080848.
835 52. Hall DR, Johnson RM, Kwon H, Ferdous Z, Laredo-Tiscareno SV, Blitvich BJ, et
836 al., Mosquito immune cells enhance dengue and Zika virus dissemination in
837 Aedes aegypti. bioRxiv, 2024. DOI: 10.1101/2024.04.03.587950.
838 53. Ramirez L, Betanzos A, Raya-Sandino A, Gonzalez-Mariscal L, and Del Angel
839 RM, Dengue virus enters and exits epithelial cells through both apical and
840 basolateral surfaces and perturbs the apical junctional complex. Virus Res, 2018.
841 **258**: p. 39-49. DOI: 10.1016/j.virusres.2018.09.016.
842 54. Gerrard SR, Rollin PE, and Nichol ST, Bidirectional infection and release of Rift
843 Valley fever virus in polarized epithelial cells. Virology, 2002. **301**(2): p. 226-35.
844 DOI: 10.1006/viro.2002.1588.
845 55. Singh VB, Singh MV, Gorantla S, Poluektova LY, and Maggirwar SB,
846 Smoothened Agonist Reduces Human Immunodeficiency Virus Type-1-Induced
847 Blood-Brain Barrier Breakdown in Humanized Mice. Sci Rep, 2016. **6**: p. 26876.
848 DOI: 10.1038/srep26876.
849 56. Doyle T, Moncorge O, Bonaventure B, Pollpeter D, Lussignol M, Tauziet M, et
850 al., The interferon-inducible isoform of NCOA7 inhibits endosome-mediated viral
851 entry. Nat Microbiol, 2018. **3**(12): p. 1369-1376. DOI: 10.1038/s41564-018-0273-
852 9.
853 57. Khan H, Winstone H, Jimenez-Guardeno JM, Graham C, Doores KJ, Goujon C,
854 et al., TMPRSS2 promotes SARS-CoV-2 evasion from NCOA7-mediated

855 restriction. PLoS Pathog, 2021. **17**(11): p. e1009820. DOI:
856 10.1371/journal.ppat.1009820.
857 58. Yaple-Maresh ME, Flores GG, Zimmerman GE, Gomez-Rivera F, and Collins KL,
858 Virus-induced vesicular acidification enhances HIV immune evasion. bioRxiv,
859 2024. DOI: 10.1101/2024.12.17.628989.
860 59. Petit MJ, Kenaston MW, Pham OH, Nagainis AA, Fishburn AT, and Shah PS,
861 Nuclear dengue virus NS5 antagonizes expression of PAF1-dependent immune
862 response genes. PLoS Pathog, 2021. **17**(11): p. e1010100. DOI:
863 10.1371/journal.ppat.1010100.
864 60. Harmon B, Bird SW, Schudel BR, Hatch AV, Rasley A, and Negrete OA, A
865 Genome-Wide RNA Interference Screen Identifies a Role for Wnt/beta-Catenin
866 Signaling during Rift Valley Fever Virus Infection. J Virol, 2016. **90**(16): p. 7084-
867 7097. DOI: 10.1128/JVI.00543-16.
868 61. Ikegami T, Narayanan K, Won S, Kamitani W, Peters CJ, and Makino S, Dual
869 functions of Rift Valley fever virus NSs protein: inhibition of host mRNA
870 transcription and post-transcriptional downregulation of protein kinase PKR. Ann
871 N Y Acad Sci, 2009. **1171 Suppl 1**(Suppl 1): p. E75-85. DOI: 10.1111/j.1749-
872 6632.2009.05054.x.
873 62. Billecocq A, Gauliard N, Le May N, Elliott RM, Flick R, and Bouloy M, RNA
874 polymerase I-mediated expression of viral RNA for the rescue of infectious
875 virulent and avirulent Rift Valley fever viruses. Virology, 2008. **378**(2): p. 377-84.
876 DOI: 10.1016/j.virol.2008.05.033.
877 63. Bonizzoni M, Dunn WA, Campbell CL, Olson KE, Dimon MT, Marinotti O, et al.,
878 RNA-seq analyses of blood-induced changes in gene expression in the mosquito
879 vector species, Aedes aegypti. BMC Genomics, 2011. **12**: p. 82. DOI:
880 10.1186/1471-2164-12-82.
881 64. Turell MJ, Wilson WC, and Bennett KE, Potential for North American mosquitoes
882 (Diptera: Culicidae) to transmit rift valley fever virus. J Med Entomol, 2010. **47**(5):
883 p. 884-9. DOI: 10.1603/me10007.
884 65. Chowdhury A, Modahl CM, Tan ST, Wong Wei Xiang B, Misse D, Vial T, et al.,
885 JNK pathway restricts DENV2, ZIKV and CHIKV infection by activating
886 complement and apoptosis in mosquito salivary glands. PLoS Pathog, 2020.
887 **16**(8): p. e1008754. DOI: 10.1371/journal.ppat.1008754.
888 66. Vera-Maloof FZ, Saavedra-Rodriguez K, Elizondo-Quiroga AE, Lozano-Fuentes
889 S, and Black IV WC, Coevolution of the Ile1,016 and Cys1,534 Mutations in the
890 Voltage Gated Sodium Channel Gene of *Aedes aegypti* in Mexico. PLoS Negl
891 Trop Dis, 2015. **9**(12): p. e0004263. DOI: 10.1371/journal.pntd.0004263.
892 67. Black WC and DuTeau NM, RAPD-PCR and SSCP analysis for insect population
893 genetic studies, in *The Molecular Biology of Insect Disease Vectors: A Methods*
894 *Manual* C.B.B.a.C.L. J. Crampton, Editor. 1997, Chapman and Hall: New York. p.
895 361–373.
896 68. Chen S, Ultrafast one-pass FASTQ data preprocessing, quality control, and
897 deduplication using fastp. Imeta, 2023. **2**(2): p. e107. DOI: 10.1002/imt2.107.
898 69. Carroll TS, Liang Z, Salama R, Stark R, and de Santiago I, Impact of artifact
899 removal on ChIP quality metrics in ChIP-seq and ChIP-exo data. Front Genet,
900 2014. **5**: p. 75. DOI: 10.3389/fgene.2014.00075.

70. Kim D, Paggi JM, Park C, Bennett C, and Salzberg SL, Graph-based genome alignment and genotyping with HISAT2 and HISAT-genotype. Nat Biotechnol, 2019. **37**(8): p. 907-915. DOI: 10.1038/s41587-019-0201-4.
71. Matthews BJ, Dudchenko O, Kingan SB, Koren S, Antoshechkin I, Crawford JE, et al., Improved reference genome of Aedes aegypti informs arbovirus vector control. Nature, 2018. **563**(7732): p. 501-507. DOI: 10.1038/s41586-018-0692-z.
72. Zhang Y, Liu T, Meyer CA, Eeckhoute J, Johnson DS, Bernstein BE, et al., Model-based analysis of ChIP-Seq (MACS). Genome Biol, 2008. **9**(9): p. R137. DOI: 10.1186/gb-2008-9-9-r137.
73. Ramirez F, Ryan DP, Gruning B, Bhardwaj V, Kilpert F, Richter AS, et al., deepTools2: a next generation web server for deep-sequencing data analysis. Nucleic Acids Res, 2016. **44**(W1): p. W160-5. DOI: 10.1093/nar/gkw257.
74. Ross-Innes CS, Stark R, Teschendorff AE, Holmes KA, Ali HR, Dunning MJ, et al., Differential oestrogen receptor binding is associated with clinical outcome in breast cancer. Nature, 2012. **481**(7381): p. 389-93. DOI: 10.1038/nature10730.
75. Team RC, R: A language and environment for statistical computing. 2021, R Foundation for Statistical Computing: Vienna, Austria.
76. Sergushichev AA, An algorithm for fast preranked gene set enrichment analysis using cumulative statistic calculation. bioRxiv, 2016: p. 060012. DOI: 10.1101/060012.
77. Subramanian A, Tamayo P, Mootha VK, Mukherjee S, Ebert BL, Gillette MA, et al., Gene set enrichment analysis: a knowledge-based approach for interpreting genome-wide expression profiles. Proc Natl Acad Sci U S A, 2005. **102**(43): p. 15545-50. DOI: 10.1073/pnas.0506580102.
78. Wang Q, Li M, Wu T, Zhan L, Li L, Chen M, et al., Exploring Epigenomic Datasets by ChIPseeker. Curr Protoc, 2022. **2**(10): p. e585. DOI: 10.1002/cpz1.585.
79. Yu G, Wang LG, and He QY, ChIPseeker: an R/Bioconductor package for ChIP peak annotation, comparison and visualization. Bioinformatics, 2015. **31**(14): p. 2382-3. DOI: 10.1093/bioinformatics/btv145.
80. Yu G and Gao C-H, enrichplot: Visualization of Functional Enrichment Result. 2025. p. R package version 1.28.4.
81. Wu T, Hu E, Xu S, Chen M, Guo P, Dai Z, et al., clusterProfiler 4.0: A universal enrichment tool for interpreting omics data. Innovation (Camb), 2021. **2**(3): p. 100141. DOI: 10.1016/j.xinn.2021.100141.
82. Heinz S, Benner C, Spann N, Bertolino E, Lin YC, Laslo P, et al., Simple combinations of lineage-determining transcription factors prime cis-regulatory elements required for macrophage and B cell identities. Mol Cell, 2010. **38**(4): p. 576-89. DOI: 10.1016/j.molcel.2010.05.004.

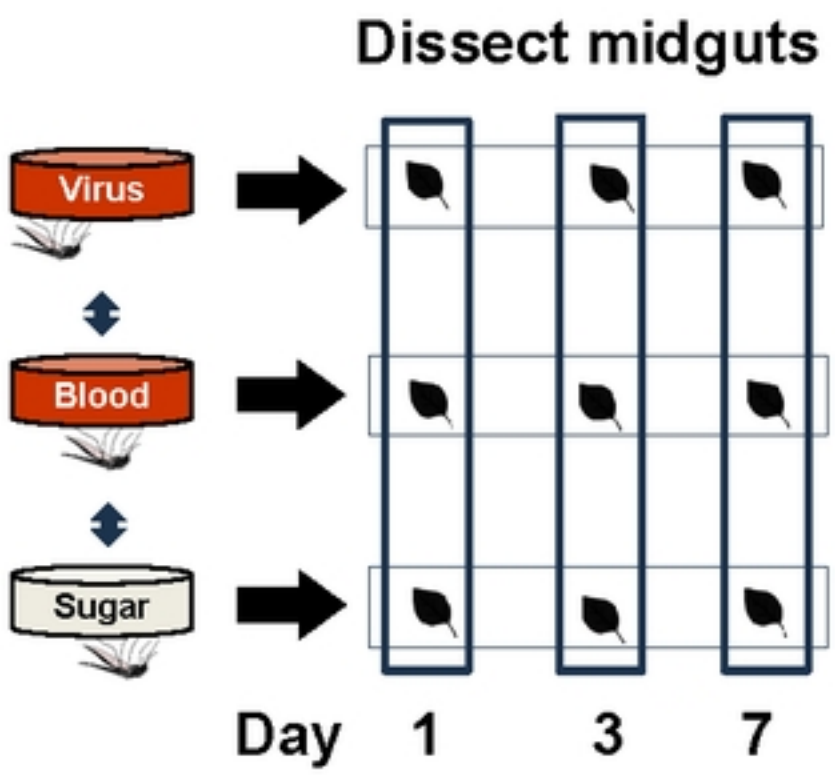

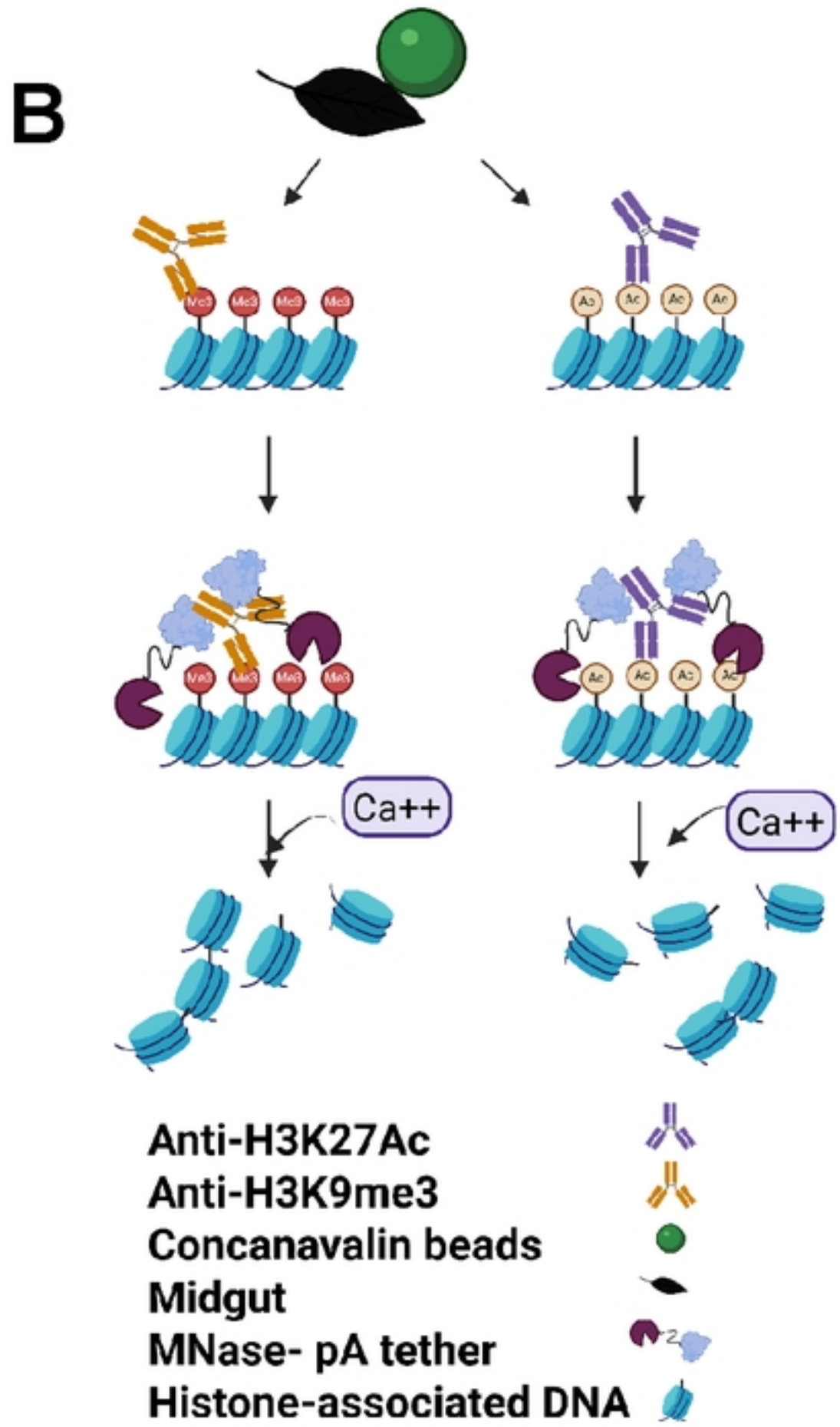

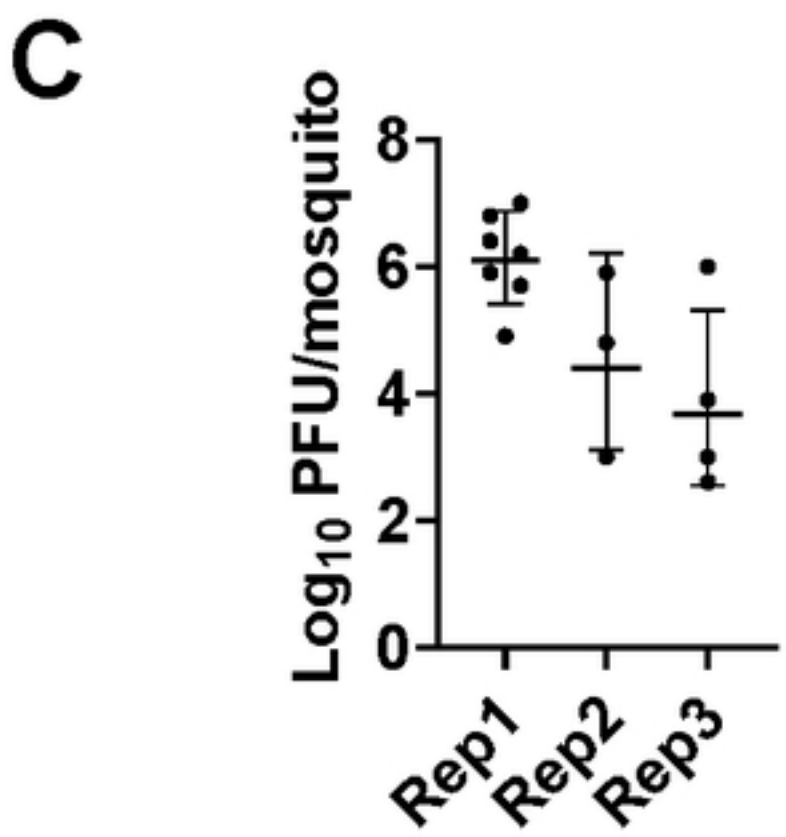

Tissue	Pos	Neg	(Total #) Infection Rate
Whole mosquitoes	15	15	(30) 50%
Carcasses- dissemination	22	58	(80) 27.5%

Fig1

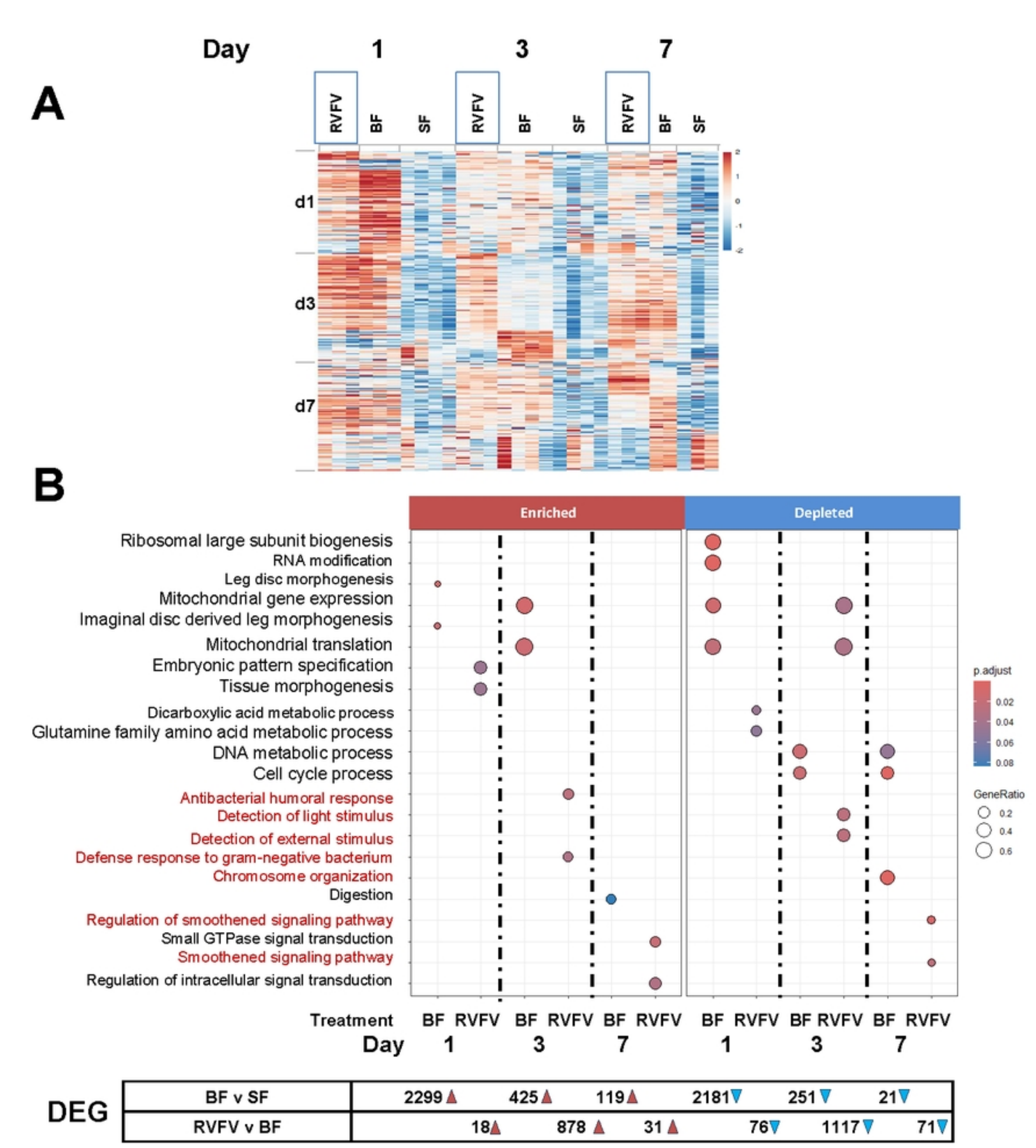
A
Day
1
3
7
RVFV
BF
SF
d1
d3
d7
B
Enriched
Depleted
Ribosomal large subunit biogenesis
RNA modification
Leg disc morphogenesis
Mitochondrial gene expression
Imaginal disc derived leg morphogenesis
Mitochondrial translation
Embryonic pattern specification
Tissue morphogenesis
Dicarboxylic acid metabolic process
Glutamine family amino acid metabolic process
DNA metabolic process
Cell cycle process
Antibacterial humoral response
Detection of light stimulus
Detection of external stimulus
Defense response to gram-negative bacterium
Chromosome organization
Digestion
Regulation of smoothened signaling pathway
Small GTPase signal transduction
Smoothened signaling pathway
Regulation of intracellular signal transduction
Treatment
BF RVFV BF RVFV BF RVFV BF RVFV BF RVFV BF RVFV
Day
1 3 7 1 3 7
p.adjust
0.02
0.04
0.06
0.08
GeneRatio
0.2
0.4
0.6
DEG
BF v SF
2299 425 119 2181 251 21
RVFV v BF
18 878 31 76 1117 71

Fig2

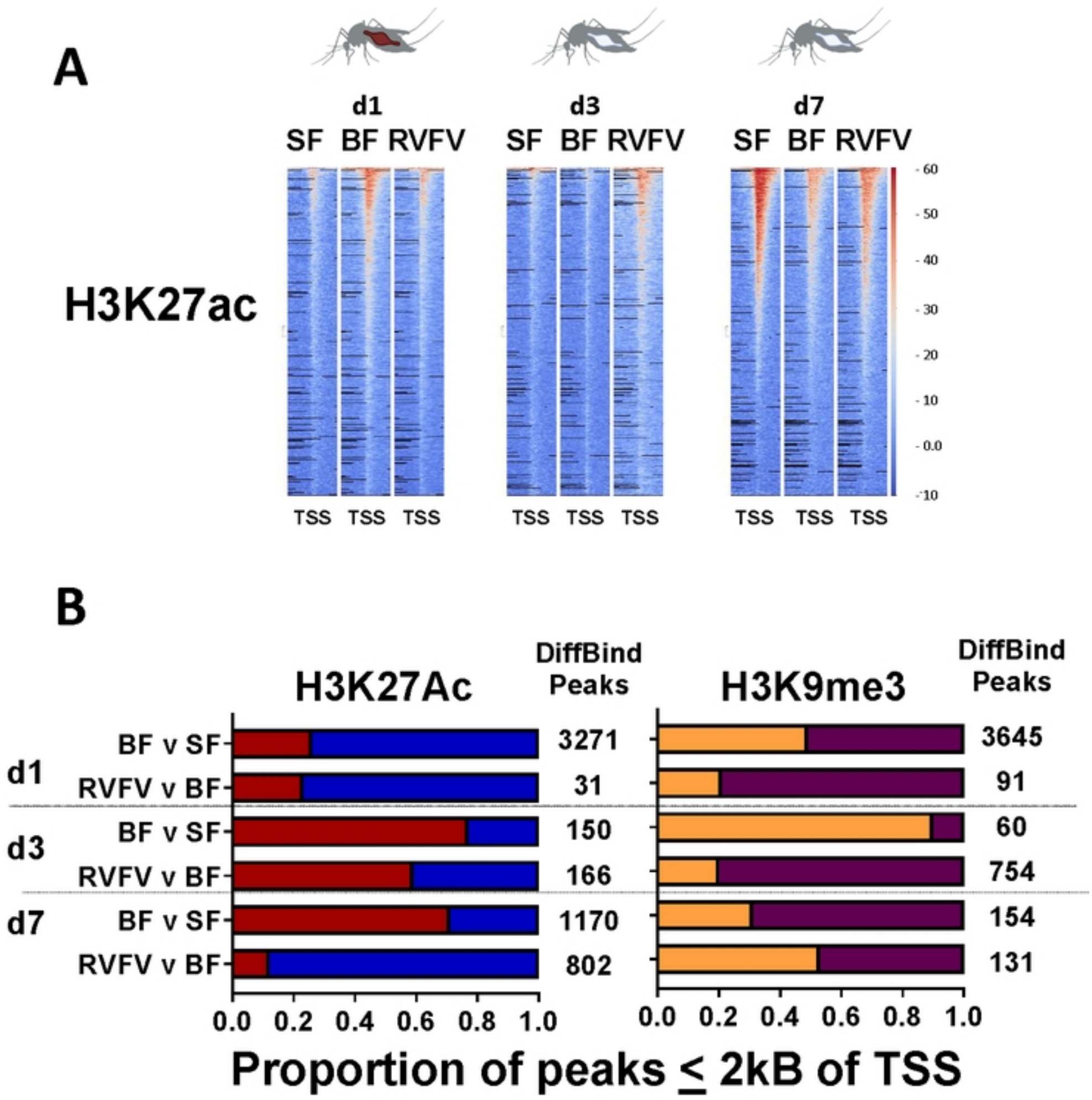
A
H3K27ac
d1
d3
d7
SF BF RVFV
TSS
- 60
- 50
- 40
- 30
- 20
- 10
- 0.0
-10
B
H3K27Ac
H3K9me3
DiffBind Peaks
BF v SF
RVFV v BF
3271
31
150
166
1170
802
3645
91
60
754
154
131
0.0 0.2 0.4 0.6 0.8 1.0
Proportion of peaks ≤ 2kB of TSS

Fig3